Direct Production of Graphene Nanosheets for Near Infrared Photoacoustic Imaging

Mehulkumar A. Patel,[†] Hao Yang,[‡] Pui Lam Chiu,[†] Daniel D. T. Mastrogiovanni,[§] Carol R. Flach,[†] Keerthi Savaram,[†] Lesly Gomez,[†] Ashley Hemnarine,[⊥] Richard Mendelsohn,[†] Eric Garfunkel,[§] Huabei Jiang,[‡,*] and Huixin He[†,*]

[†]Chemistry Department, Rutgers University, Newark, New Jersey 07102, United States, [‡]J. Crayton Pruitt Family Department of Biomedical Engineering, University of Florida, JG56BMS Building, Gainesville, Florida 32611, United States, [§]Department of Chemistry and Chemical Biology, Rutgers University, 610 Taylor Road, Piscataway, New Jersey 08854, United States, and [⊥]Science Park High School, 260 Norfolk Street, Newark, New Jersey 07103, United States

ABSTRACT Hummers method is commonly used for the fabrication of graphene oxide (GO) from graphite particles. The oxidation process also leads to the cutting of graphene sheets into small pieces. From a thermodynamic perspective, it seems improbable that the aggressive, somewhat random oxidative cutting process could directly result in graphene nanosheets without destroying the intrinsic π-conjugated structures and the associated exotic properties of graphene. In Hummers method, both $KMnO_4$ and NO_2^+ (nitronium ions) in concentrated H_2SO_4 solutions act as oxidants *via* different oxidation mechanisms. From both experimental observations and theoretical calculations, it appears that $KMnO_4$ plays a major role in the observed oxidative cutting and unzipping processes. We find that $KMnO_4$ also limits nitronium oxidative etching of graphene basal planes, therefore slowing down graphene fracturing processes for nanosheet fabrication. By intentionally excluding $KMnO_4$ and exploiting pure nitronium ion oxidation, aided by the unique thermal and kinetic effects induced by microwave heating, we find that graphite particles can be converted into graphene nanosheets with their π-conjugated aromatic structures and properties largely retained. Without the need of any postreduction processes to remove the high concentration of oxygenated groups that results from Hummers GO formation, the graphene nanosheets as-fabricated exhibit strong absorption, which is nearly wavelength-independent in the visible and near-infrared (NIR) regions, an optical property typical for intrinsic graphene sheets. For the first time, we demonstrate that strong photoacoustic signals can be generated from these graphene nanosheets with NIR excitation. The photo-to-acoustic conversion is weakly dependent on the wavelength of the NIR excitation, which is different from all other NIR photoacoustic contrast agents previously reported.

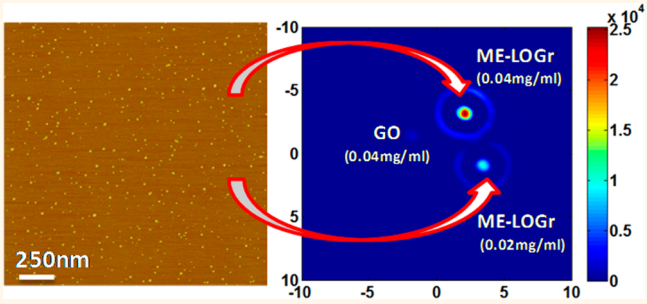

KEYWORDS: graphene nanosheets · photoacoustic imaging · nitronium ions · oxidation · microwave chemistry · graphene oxides (GO)

Recently, there has been a surge of interest in nanosized graphene sheets due to their unique size effects,[1−4] edge effects,[5−7] and even quantum confinement effects,[8] in addition to the intrinsic exotic properties of graphene. Several strategies have been developed to fabricate nanosized graphene sheets.[8−10] Most of them rely on chemical oxidation *via* Hummers method or other modified Hummers methods, which always involve the oxidization of graphite powder to produce heavily oxidized graphene sheets termed graphene oxide (GO).[11] The oxidation reaction is a lengthy process (from hours to several days), and the aggressive chemistry also leads to uncontrollable cutting/unzipping of graphene sheets into small pieces of different sizes and shapes with extensive defects.[12,13]

To reach predefined nanometer-sized GO sheets, extended oxidation and sonication[14] or other oxidative cutting reactions are required.[10,15] Alternatively, nanosized GO sheets can be synthesized using starting materials which are already small such as graphite nanofibers or carbon fibers.[16,17] In GO, most of the exotic properties of graphene have vanished due to the high density of oxygen-containing groups that heavily distort and break up the π-conjugated structure.

* Address correspondence to huixinhe@rutgers.edu, hjiang@bme.ufl.edu.

Received for review July 5, 2013 and accepted August 22, 2013.

Published online August 23, 2013
10.1021/nn403429v

Various approaches to reduce GO including chemical, electrochemical, and hydrothermal methods have been explored with only a fraction of the graphene properties recovered.[4,8,9,18−20] No strategy has been reported to directly fabricate graphene nanosheets (instead of GO nanosheets) in a one-pot reaction. Theoretical studies of graphite oxidation have demonstrated that the activation barrier to initiate the oxidation of pristine graphene is much greater than the energy requirement for additional oxidation at those defect sites.[21] It is the latter oxidation process that is responsible for cutting graphene sheets into small pieces.[1,22,23] Therefore, from a thermodynamic point of view, it is a daunting challenge to directly produce graphene nanosheets (instead of graphene oxide) with their π-conjugated structures, and properties of graphene largely retained in a one-pot oxidation reaction.[23]

Microwave chemistry, because of the different heating mechanism compared to traditional convection heating, has been well-known for high speed synthesis, shortening reaction times from days to minutes, even to seconds.[24] Even though the observed rate enhancements have been ascribed to purely thermal/kinetic effects, *i.e.*, a consequence of the high reaction temperatures that can be attained so rapidly, these unique effects can also lead to reaction selectivity to enable fabrication of desired products.[25] Herein we report an unexpected discovery that monodispersed graphene nanosheets can be directly and rapidly (30 s) fabricated *via* microwave-assisted nitronium oxidation chemistry. The graphene nanosheets as-fabricated have strong NIR absorption and high efficiency in the generation of photoacoustic signals without the need of any post-reduction processes. Furthermore, from previous experimental reports on the oxidation of carbon nanotubes (CNTs)[1,22,23] and recent theoretical studies on the mechanism of graphene unzipping/cutting,[13,26] it can be concluded that $KMnO_4$ in Hummers method plays a major role in the experimentally observed cutting/unzipping. We reveal that $KMnO_4$ may also protect the already oxidized sites from gasification (CO_2 and/or CO) and hole generation, and thereby slow down the subsequent global fracture of graphene sheets into nanosized pieces. At the same time, $KMnO_4$ may also initiate its own oxidative cutting leading to highly oxidized graphene sheets with much larger lateral dimensions and straight edges compared to graphene nanosheets obtained *via* nitronium oxidation. Understanding the roles and molecular cutting mechanisms of these oxidants allows us to fabricate graphene sheets in a controlled fashion with different morphological and electronic structures to accommodate different applications.

RESULTS AND DISCUSSION

We recently developed a rapid, microwave-enabled, scalable approach to produce large, highly conductive graphene sheets directly from graphite powder.[27] We intentionally excluded $KMnO_4$ (as is used in Hummers methods) with the aim of avoiding cutting and exploited the advantage of aromatic oxidation by nitronium ions (NO_2^+) combined with microwave heating. This unique combination promotes rapid and simultaneous oxidation of multiple non-neighboring carbon atoms across an entire graphene sheet, so that a minimum concentration of oxygen moieties enables the separation and dispersion of relatively large graphene sheets (several tens of micrometers) into solutions without cutting them into small pieces.[27] Because of the essential role of microwave heating during the production, we refer to these dispersed graphene sheets as microwave-enabled low oxygen graphene (ME-LOGr). High resolution transmission electron microscopy shows that the ME-LOGr consists of many different crystalline-like domains, which are uniformly distributed across the entire ME-LOGr sheets.

In this work, we discovered that high concentrations of graphene nanosheets can be rapidly obtained by simply increasing the NO_2^+ concentration. In a typical experiment, graphite powder is mixed with concentrated nitric acid, sulfuric acid, and a small amount of water (volume ratio of HNO_3:H_2SO_4:H_2O of 1:2.5:0.07), and then the solution was subjected to 30 s of microwave irradiation (300 W). The reaction results in a dispersed slurry, which is significantly easier to clean and handle than the sticky paste obtained from Hummers method.[11] Vacuum filtration was used to remove the acid residues and the possible byproducts. With the help of bath sonication (30 min), the cleaned cake on the filter paper can be redispersed in a wide range of polar solvents to form graphene colloidal solutions without the use of surfactants or stabilizers. The concentration of the nanosheets in water is 0.4 mg/mL, and is much higher in other organic solvents, such as *N*,*N*-dimethylformamide (DMF), acetone, pyridine, and acetonitrile (Supporting Information, Figure S1). These solutions are stable, showing no precipitation for several months. From atomic force microscopy (AFM) measurements (Figure 1A), the nanosheets have a lateral diameter of 10 ± 4 nm and an average thickness of 0.75 ± 0.23 nm (see statistical analysis in Supporting Information, Figure S2). This result demonstrates that the microwave-assisted oxidation reaction directly converted the large graphene sheets in graphite particles into graphene nanosheets with a thickness of one or two layers, which is in stark contrast to previous approaches that require a separate step for cutting the GO sheets to the nanometer scale.[14,15]

The color of the nanosheet suspensions is grayish black, similar to the suspensions of the larger ME-LOGr sheets,[27] which qualitatively suggests that we have directly obtained graphene nanosheets with small amounts of oxygen-containing groups instead of heavily oxidized GO nanosheets (Figure 1B, inset). The plasmon band in the UV region (Figure 1B) is centered

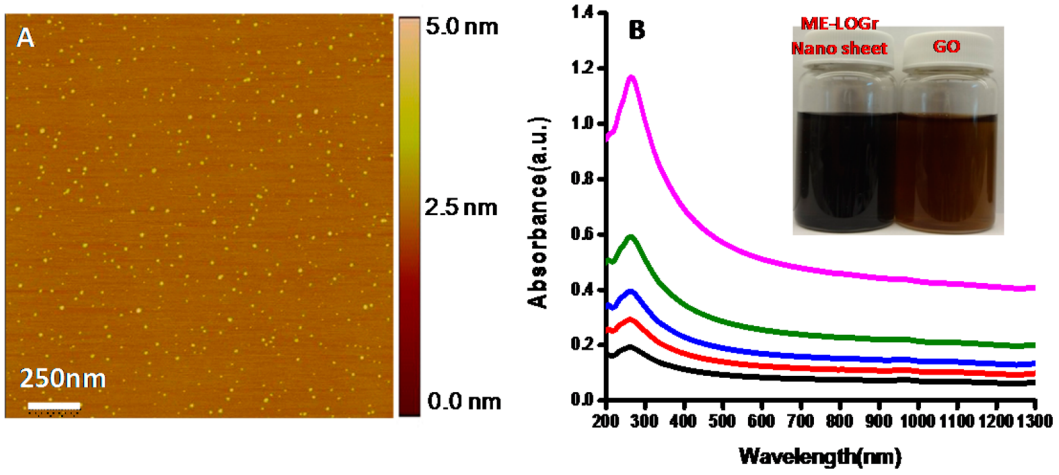

Figure 1. (A) AFM images of ME-LOGr nanosheets, (B) UV−vis−NIR spectra of ME-LOGr nanosheets with concentrations of 20 (pink), 10 (olive), 6.7 (blue), 5 (red), and 3.3 mg/L (black), respectively. Inset B, a digital picture of an aqueous suspension of ME-LOGr nanosheets (left) and graphene oxide (GO) nanosheets (right) shows different colors, indicating they are in different oxidation states. The GO nanosheets were obtained *via* control-A experiment in which nitronium ions and $KMnO_4$ both act as an oxidant.

at ~262 nm, slightly blue-shifted compared to the larger ME-LOGr sheets (267 nm), but still much higher than GO (~230 nm).[28] Additionally, unlike GO, the UV−vis−NIR spectrum of the solution of graphene nanosheets displayed strong while nearly wavelength-independent absorption in the visible and NIR regions, which suggests that the π-conjugation within the graphene sheets is largely retained.[29−31] The molecular absorption coefficient of the nanosheets at 984 nm is 21.7 L/g·cm and at 808 nm is 22.7 L/g·cm, which is very close to that of reduced GO (rGO) nanosheets (24.6 L/g·cm at 808 nm) as reported by Dai *et al.*[19] It should be noted that the molecular absorption coefficient of the rGO nanosheets was measured after they were pegylated because of the insolubility of rGO in aqueous solutions.

The chemical functionalities of the nanosheets were studied with X-ray photoelectron spectroscopy (XPS) (Figure 2). The nanosheets have a large amount of carbon that is not bound to oxygen (~80% of the total carbon), similar to the larger-sized ME-LOGr sheets,[27] and those of reduced GO sheets.[32,33] Because of the similar production procedures and oxidation levels of the larger-sized ME-LOGr sheets, we refer to these nanosheets as ME-LOGr nanosheets. With careful fitting, we found that the nanosheets contained more oxygen functional groups of higher oxidation levels, such as −COOH, than was observed in larger ME-LOGr sheets.[27] This is consistent with the observation that −COOH groups are normally located on the edges of the graphene sheets.[34,35] The nanosheets obviously contain a higher edge/center ratio when compared to larger ME-LOGr sheets.

Even though the ME-LOGr nanosheets contain a similar quantity of oxygen-free carbon compared to that reported for rGO,[32−34] they may have different molecular structures, which leads to different physical and chemical properties. As an example, most of the

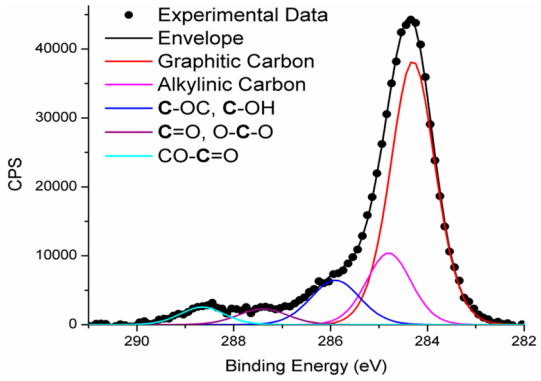

Figure 2. An X-ray photoelectron spectrum (XPS) of ME-LOGr nanosheets.

rGO sheets are not stable in aqueous solution without the help of surfactants or stabilizers. Furthermore, it was reported that GO and rGO nanosheets obtained *via* further oxidation and/or reduction of large GO sheets fabricated by Hummers method are highly luminescent, which has been attributed to special edge effects and/or the existence of small and isolated graphene domains.[34,36−39] In contrast, ME-LOGr nanosheets can form stable aqueous colloidal solutions without the necessity of surfactants and stabilizers (Supporting Information, Figures S1). They are not photoluminescent, suggesting that either the intact graphene domains are much larger than those in GO or rGO nanosheets, or they possess different electronic structures at their edges.[39]

Raman spectroscopy was utilized to estimate the intact graphene domain sizes in the ME-LOGr nanosheets. The typical features of G band, defect D band, and 2D band are shown in the Raman spectrum of ME-LOGr (Figure 3). The D to G band intensity ratio (I_D/I_G) is 0.65, which is slightly higher than that from larger ME-LOGr as we reported earlier,[27] but much

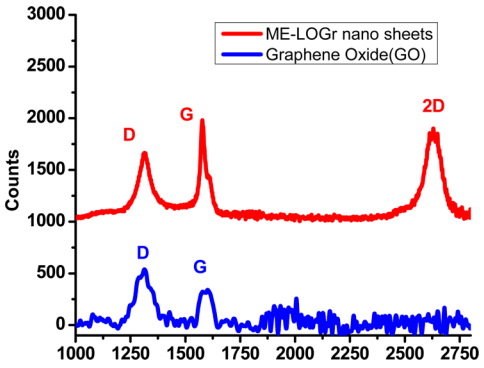

Figure 3. Raman spectra of ME-LOGr nanosheets (red) and GO nanosheets (blue). GO nanosheets were obtained *via* control-A experiment where nitronium ions and $KMnO_4$ both act as an oxidant.

lower than GO (1.65). The reported I_D/I_G ratios for rGO are similar to, or even higher than that for GO, which has been explained by the fact that chemical reduction preferentially generates a greater number of smaller crystalline domains rather than increasing the size of existing graphitic domains.[40,41] Using the empirical Tuinstra−Koenig relation,[42] we estimated that the size of the ordered crystallite graphitic domains was ≈6.7 nm, much larger than those in GO and rGO (1−3 nm). Therefore, although the apparent electronic structure and the graphitic carbon components of the ME-LOGr nanosheets are similar to rGO, as demonstrated by their color, UV−vis−NIR and XPS spectra, the ME-LOGr sheets have unique molecular structures that differ from both GO and rGO.[41,43]

It has been reported that the 2D band in GO is absent.[33,41] Additionally, the reduction of GO results in only a small increase in the 2D band intensity, presumably due to the defects in the graphitic structures.[40] A decrease of the 2D band intensity has also been associated with the modification of pristine graphene through chemisorption[44] and physisorption.[45,46] However, for ME-LOGr nanosheets, the intensity of the 2D band is similar to that of the G band. The small intensity ratio of D/G bands and the high intensity of 2D band are in contrast to the larger D/G band ratio and the absence of the 2D band in GO and rGO, indicating that the intrinsic structure and properties of graphene were largely retained in ME-LOGr nanosheets, and these nanosheets are clean without adsorbent-induced surface modification.[40]

All of these results collectively demonstrate that microwave heating and nitronium oxidation of graphite particles directly leads to relatively "clean" graphene nanosheets instead of GO nanosheets as produced *via* Hummers method.[11] The molecular mechanism for the experimentally observed graphite oxidation and the accompanied graphene sheet cutting *via* Hummers method remains elusive. From density functional calculations, it has been reported that graphene cutting is likely initiated by the formation of an epoxy group. The strain associated with epoxy group formation on graphene facilitates the generation of another epoxy group at its nearest neighbor, and finally leads to linearly aligned epoxy groups on the surface as the oxidation progresses.[13,26,47] These aligned epoxy groups co-operatively strain the graphene sheets, which account for the GO cutting. In Hummers method, both HNO_3 and $KMnO_4$ in concentrated H_2SO_4 act as oxidants *via* different mechanisms ($NaNO_3$ converts to HNO_3 under acidic conditions),[11] so it is not immediately clear which oxidant played a more important role in the observed graphene sheet cutting.

Because of the chemical similarity of graphene and carbon nanotubes (CNTs), additional insight into the mechanism of oxidative cutting of graphene/GO sheets may also be derived from the extensive experimental studies of shortening and longitudinal unzipping of CNTs. Both $KMnO_4/H_2SO_4$ and HNO_3/H_2SO_4 have been used for oxidative cutting of CNTs. An important common feature for these two oxidation systems is that the initiation, which produces various oxygen-containing groups, is the rate determining step. Further local oxidation of the oxidized carbon atoms and their near neighbors(the key procedure in cutting and unzipping) under the same reaction conditions is favored over oxidation on defect-free graphene regions in these two cases.[23] Both methods produced highly oxidized products, indicating that further oxidation of the defect-free graphene regions is still continuing during the cutting step.[1,22,48]

While the oxidation processes that occur *via* nitronium ions (produced by the mixture of concentrated HNO_3 and H_2SO_4) lead mainly to CNT shortening,[22,48] the oxidation by $KMnO_4$ in anhydrous H_2SO_4 predominantly induces longitudinal unzipping of CNTs to produce graphene nanoribbons.[1] It was reported that nitronium ions not only attack the existing defects on the graphene, but also randomly attack the relatively inert defect-free graphene basal planes, producing various oxygen-containing groups,[1] which is the first step in oxidative cutting. As the oxidation progresses, it can further etch these oxidized sites, leading to vacancies, holes, and finally fracturing the CNTs into short pieces.[22,48] The mechanism for the longitudinal unzipping has been explained by the oxidation being initiated with permanganate ions attacking predominantly existing defects in CNTs (such as alkenes) to form a cyclic manganate ester. With further oxidation, the esters can form dione structures, which distort the β,α-alkenes making the neighboring sites more prone to further attacks. It is in this stepwise manner that the longitudinal unzipping of the tubes into ribbons occurs. Note that most of the GO sheets formed *via* Hummers methods have straight edges[29] similar to the graphene ribbons obtained by longitudinal unzipping of CNTs *via* $KMnO_4/H_2SO_4$. Combined with the theoretical studies described above,[13,26] it is easy to conclude that $KMnO_4$ plays a major role in the observed cutting/unzipping in Hummers oxidation processes.

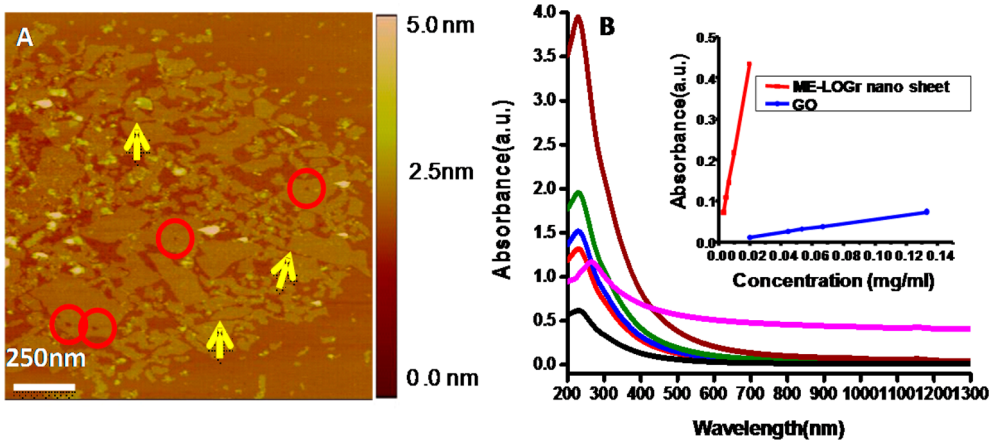

Figure 4. (A) AFM images of graphene oxide nanosheets obtained *via* control-A experiment. Some of the nanometer gaps between nanosheets and nanoholes generated during the oxidation reaction were labeled with arrows and circles, respectively. (B) UV−vis−NIR spectra of the GO sheets at different concentrations of 133.3 (wine), 66.7 (olive), 53.3 (blue), 44.4 (red), and 33.3 mg/L (black), respectively. For better comparison, the pink curve (20 mg/L of ME-LOGr nanosheets) in Figure 1B is also displayed in panel B with the same color. Inset (B) shows the linear relationships between the absorption at 984 nm and the concentration of ME-LOGr nanosheets and GO. The mass coefficient of the ME-LOGr is 40 fold higher than that of GO.

As a control experiment (which is referred as control-A), $KMnO_4$ (5 times of the weight of graphite particles, the same ratio has been used to unzip CNTs[1]) was introduced to the reaction mixture with the same previously used volume ratio of $H_2SO_4/HNO_3/H_2O$ (which we assume, to first order, will result in the same concentration of nitronium ions in solution). Applying the same microwave power and irradiation time, a highly oxidized product is obtained. Similar vacuum filtration procedures were performed to clean the residues of $KMnO_4$, acids, and other reaction byproducts. The resulting filtrate cake appeared quite similar to GO prepared by traditional Hummers methods and was sticky and time-consuming to clean.[49] When the cleaned filtrate cake was redispersed into water solution, the dispersed solution showed a brownish color (Figure 1B inset). The plasmon band of the control suspension in the UV region is centered at ~230 nm (Figure 4B), similar to that of GO prepared by Hummers method.[50] The absorption in the visible and NIR region dramatically decreased. The mass absorption coefficient at 808 and 984 nm decreased to 0.76 and 0.54 L/g·cm, respectively. Compared to the ME-LOGr nanosheets at the same wavelengths (22.7 and 21.78 L/g·cm, respectively), this represents more than 30 and 40-fold decreases, suggesting that the addition of $KMnO_4$ to the system caused extensive oxidation of the graphene sheets. The much larger D/G ratio (1.65) and the complete absence of the 2D band in the Raman spectrum shown in Figure 3 provided further evidence that the product was heavily oxidized.

Surprisingly, the size of the control sheets is much larger than the ME-LOGr nanosheets obtained without $KMnO_4$ present (Figure 4A). We observe a significant proportion of sheets in the range of 200−400 nm among smaller sheets of several tens of nanometers. Additionally, a large majority of the sheets have straight edges, quite similar to GO sheets obtained *via* Hummers method. For the first time, we observed some GO sheets with straight edges separated with small gaps of only several nanometers (indicated by arrows in Figure 4A). These nanogaps provide strong evidence that molecular cutting/unzipping has occurred during the oxidation. Since these nanogaps are only observed when $KMnO_4$ is present during the reaction, it is apparent that $KMnO_4$ plays a major role in cutting and unzipping graphene sheets to small pieces, similar to those observed in Hummers method.[13]

To further understand the role of $KMnO_4$ as the sole oxidant, another control experiment (referred as control-B) was conducted. In this experiment, NO_2^+ was excluded, and the same weight ratio (5:1) between $KMnO_4$ and graphite particles in H_2SO_4 was used. Applying the same microwave power and irradiation time, Similar to the product obtained with both $KMnO_4$ and NO_2^+ (control-A), the dispersed graphene sheets were highly oxidized in the reaction mixture, indicated by its yellowish-brownish color, and the maximum absorption at 235 nm in its UV−vis spectrum (Supporting Information, Figure S4A). However, the concentration of the dispersed sheets is about 10 times lower than that achieved in control-A. Furthermore, a large majority of the dispersed sheets are multiple layered as observed by AFM measurements (Supporting Information, Figure S4B). Most of the graphite particles were not exfoliated, and they settled on the bottom of the vial, suggesting that the capability of $KMnO_4$ in anhydrous H_2SO_4 to intercalate into and oxidize the inner parts of graphite is not as efficient as NO_2^+ ions.

The molecular mechanisms leading to these significantly different results need further study. We hypothesize that it is due to the different initiation oxidation capabilities and the following oxidization pathways of

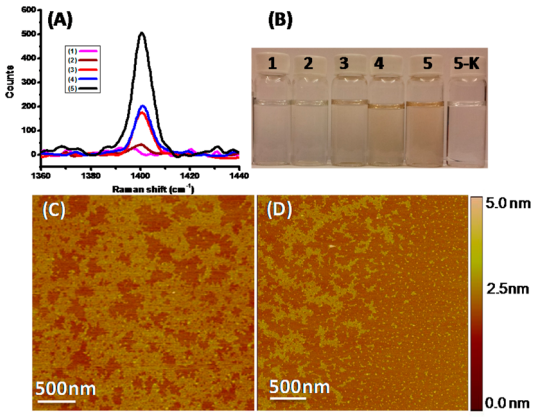

Figure 5. (A) Raman spectra of different concentrations of nitronium ions produced with different ratios of concentrated HNO_3, H_2SO_4, and H_2O with ratios of (1) 1:1:0, (2) 1:42:7, (3) 1:2.5:0.07, (4) 1:17.5:1.5, and (5) 1:4:0, respectively. (B) Digital pictures of filtrates obtained after graphite particles were oxidized in microwave with different ratios of HNO_3:H_2SO_4:H_2O of (1) to (5), and therefore different concentrations of nitronium ions. 5-K was obtained with the same ratio as (5), except that $KMnO_4$ was included. (C and D) AFM images of porous graphene sheets dispersed with magnetic stirring instead of sonication to avoid sonication-induced tearing. The graphene sheets in panels C, and D were obtained with ratio (3) and (4), respectively.

$KMnO_4$ and NO_2^+. Nitronium ions not only attack the existing defects on the graphene, but also randomly attack the relatively inert defect-free graphene basal planes.[1] In the following oxidation step, NO_2^+ continues to attack the already oxidized carbon atoms and carbon atoms far away from those already oxidized. An important consequence of these differences is that oxidation by NO_2^+ can naturally produce intact graphene domains separated by regions of oxygen-containing groups.[27] With the increased speed of the second etching step, nanosheets with retained structures can be obtained. Alternatively, $KMnO_4$ starts oxidation at existing defect sites, and the following oxidation preferentially attack the neighboring carbons, which are already oxidized. While the high temperature reached by microwave heating selectively speeds up the cutting/unzipping process, the unzipped sheets are still more oxidized.

To understand the formation pathways of graphene nanosheets *via* nitronium oxidation under microwave irradiation, different concentrations of nitronium ions were used for the microwave oxidation. The microwaved product was dispersed with mild magnetic stirring to avoid sonication-induced tearing. In our previous report, a much lower concentration of nitronium ions (Figure 5A, line 1, volume ratio of H_2SO_4:HNO_3:H_2O = 1:1:0) was used during microwave-assisted oxidation. The graphene sheets obtained were large and free of nanometer sized holes.[27] In this work, different concentrations of nitronium ions were produced with different ratios of H_2SO_4, HNO_3, and H_2O. Raman spectroscopy was used to measure the relative concentrations of the nitronium ions as the solution ratios change (Figure 5A, and Supporting Information, Figure S3).[51] With a high concentration of nitronium ions, a large number of holes were generated in the basal plane of the graphene sheets (Figure 5C). These large porous sheets were obtained using the same oxidation conditions (line 3 in Figure 5A) as those shown in Figure 1A. With further increasing the concentration of nitronium ions, more holes were generated with some of the holes becoming much larger. Eventually, the big sheets fractured into nanosized sheets. (Figure 5D). At the same time, we also found that the weight of the cleaned filtrate cake on the filter paper gradually decreased, and the color of the filtrate gradually changed from colorless to light yellow and brown (Figure 5B), indicating a large amount of carbon lost either in the form of small organic compounds or CO_2, as previously reported.[32] In contrast, when $KMnO_4$ was introduced into the reaction system, the filtrate was almost colorless (Figure 5B, vial 5-K), suggesting that much less carbon was lost during oxidation. At the same time, we found that the sheets have fewer holes (Figure 4A indicated by circles), suggesting that $KMnO_4$ protects the graphene sheets from being damaged by hole formation.

To understand the mechanism of nitronium oxidation under microwave irradiation, a control experiment (referred as control-C) was performed using the same concentration of nitronium ions (line 3 in Figure 5A), however, this time with traditional heating. The temperature was controlled at 85 °C by a water bath as reported for CNT oxidative cutting.[22,48] As expected, 30-s heating did not lead to any observable reaction. When the reaction time was extended to 4 h, small uniform graphene nanosheets (15 ± 5.3 nm in diameter and 1.5 ± 0.6 nm in height) were observed by AFM (Supporting Information, Figure S5A). When compared to the nanosheets produced with microwave heating for 30 s, these nanosheets show an additional plasmon band at 235 nm in the UV−vis spectrum (Figure S5B). This is an indication that the nanosheets are oxidized to a greater extent, which is consistent with previous reports showing that nitronium ions cut carbon nanotubes into highly oxidized short pipes.[22,48]

The exact mechanism behind these results remains inconclusive. On the basis of the observations, we assume that microwave heating changes the relative speeds of the various competitive parallel (and sequential) reactions that can occur during graphite oxidation (Figure 6). It has been reported that nitronium ions interact with graphene surfaces to form multiple aromatic radical-ion pairs *via* a single electron transfer (SET) pathway.[52] Epoxy and/or −OH groups are then formed following oxygen transfer to the aromatic radicals.[27,53] Further oxidation includes two simultaneous and competing processes: (1) continued initiation of oxidation in the intrinsic graphene domains resulting in generation of more −OH and/or

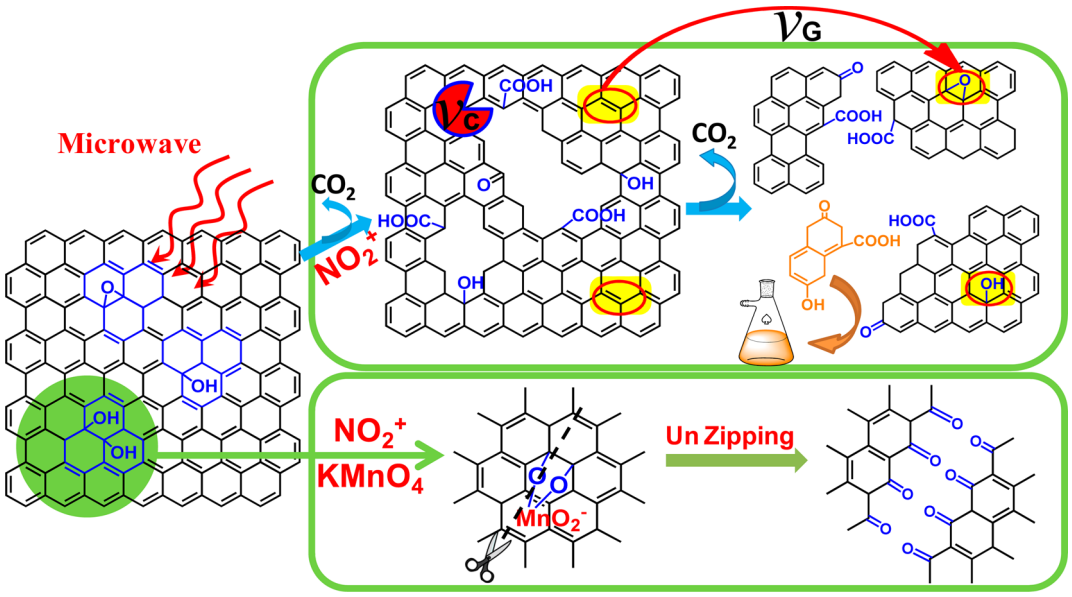

Figure 6. Schematic of the possible cutting mechanisms by microwave-assisted nitronium oxidation in the presence and absence of $KMnO_4$. v_C and v_G are referred to $v_{consumption}$ (reaction rate of defect consumption) and $v_{generation}$ (reaction rate of defect generation), respectively.

epoxy groups with a reaction rate of $v_{generation}$; and/or (2) further oxidation of the initially oxidized carbon atoms, ultimately leading to gasification of the carbon atoms (mostly CO or CO_2) and generation of small carbon residual species (which are separated during filtration), resulting in vacancies and holes throughout the graphene basal planes. This process is also called defect consumption or etching[23,54] with a reaction rate of $v_{consumption}$. It was consumption of the defects and generation of vacancies and holes in the sidewalls of carbon nanotubes that led to rapid cutting of the CNTs into short pipes and cutting graphene sheets to small pieces.[22,23] The relative reaction rates of these two processes determine the overall speed of nanosheet fabrication and also the oxidation level of the nanosheets.

Because of the strong microwave absorption characteristic of graphite particles, microwave heating leads to rapid achievement of high temperatures localized on or near the graphite particles, which in turn dramatically increases the intercalation rate of nitronium ions into the graphite particles. This process is accompanied by the generation of a large amount of −OH and/or epoxy groups distributed over the entirety of the graphene sheets (high $C_{defects}$). In the subsequent competing reactions, it is possible that the defect consumption or etching speed ($v_{consumption}$) becomes faster than that of the continuing generation of additional new defects ($v_{generation}$) on the intact graphene domains due to the high density of the −OH and/or epoxy groups generated in the first step (high $C_{defects}$).[32] With the high temperatures obtained by microwave heating, the $v_{consumption}$ may be further increased compared to $v_{generation}$ due to the lower activation barrier of the defect consumption process compared to the generation of new defects.[21] As a result, the graphene sheets are fractured into small pieces with the intrinsic structures of graphene within the pieces left largely intact (see more detailed discussion in Supporting Information).

When $KMnO_4$ is present, microwave heating also dramatically speeds up the overall oxidation processes, shortening the production times from days to tens of seconds compared to Hummers method. However, the permanganate ions possibly bind some of the epoxy groups generated by the nitronium ions, which slows down further oxidation-induced defect consumption events. As a consequence, $KMnO_4$ essentially slows down the overall speed in the production of nanosized sheets (Figure 4A). On the other hand, it may start oxidation processes following its own molecular cutting mechanism, thereby generating smaller pieces of graphene oxide sheets with straight edges.[1] Understanding these oxidative mechanisms with different oxidants allows us to controllably fabricate graphene sheets with different dimensions and electronic structures to accommodate a variety of applications.

Inspired by the strong near-infrared (NIR) absorption, high photothermal conversion efficiency, and the exceptionally large surface area of graphene, graphene nanosheets have emerged as a new high-potential nanomaterial for biological applications,[55,56] especially in the areas of photothermal therapy including photothermal enhanced drug and gene delivery systems.[18,56−59] It would be highly desirable to monitor the *in vivo* distribution of multifunctional drug delivery systems, evaluate their post-treatment therapeutic outcomes *in situ*, and most importantly, to track the long-term fate of graphene sheets in the human body. These capabilities could largely

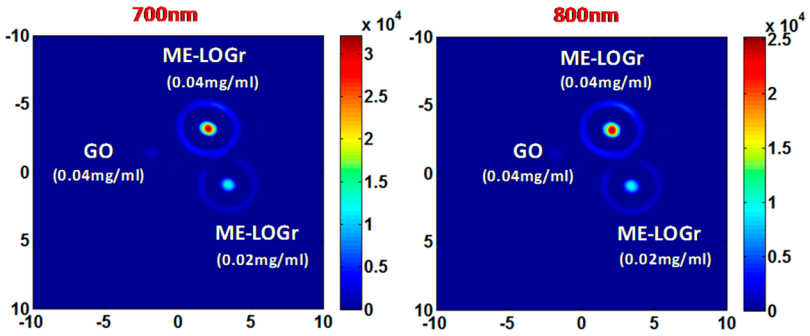

Figure 7. Photoacoustic (PA) signal of GO and graphene nanosheets of different concentrations, illuminated with 700 and 800 nm laser. The color coded vertical bar represents the strength of the photoacoustic signal generated. GO nanosheets were obtained *via* control-A experiment.

facilitate their application in practical multifunctional nanomedicine regimes, fighting various diseases.

To study the *in vivo* behavior of pegylated GO nanosheets, fluorescent and radio labeling have been used.[57] However, the fluorescent quenching in liver and spleen has led to overestimated tumor targeting efficiency. The radio-labeling method has been considered to be more reliable and accurate than fluorescence imaging but still suffers from long-term stability problems.[4,60] To unambiguously determine their long-term fate, graphene with different structures has been developed and rendered intrinsically fluorescent in the blue, green, and NIR regions for *in vitro* and *in vivo* imaging.[36,61] However, their practical applications will be limited by the low penetration depth of optical imaging methods in general.

Photoacoustic imaging (PAI), is a novel, hybrid, and noninvasive imaging modality that combines the merits of both optical and ultrasonic methods.[62] PAI, especially in the NIR region, where the attenuation of light by blood and soft tissue is relatively low, provides considerably greater spatial resolution than purely optical imaging in deep tissue while simultaneously overcoming the disadvantages of ultrasonic imaging regarding both biochemical contrast and speckle artifacts. This method could evaluate drug delivery efficiency and therapeutic effects with a relatively high spatial resolution in biological tissue.

To generate PA signals with NIR light excitation, the following conditions should be satisfied: strong NIR absorption, non-radiative relaxation, heating, and acoustic wave generation. The ME-LOGr nanosheets exhibit strong and wavelength-independent absorption in the visible and NIR regions. Their absorption (with a coefficient of 22.7 L/g·cm at 808 nm) exceeds the best NIR fluorophores (for example, indocyane green has an absorption coefficient of 13.9 L/g·cm at 808 nm) and the endogenous cellular background. The difference in NIR absorption between the graphene sheets and the background provides excellent optical confinement for PAI imaging applications.[63] Furthermore, graphene nanosheets are not luminescent, so that all the optical energy absorbed would transform to heat, which can be used for acoustic wave generation. Therefore, it is reasonable to assume that a strong NIR PA signal could be generated from these graphene nanosheets upon NIR illumination. We should mention that no study has been reported to date on the PA properties of graphene, except for a recent work by Liu *et al.*, which demonstrated that rGO nanosheets anchored with magnetic nanoparticles could be used for PA imaging.[64]

Figure 7 shows that the ME-LOGr nanosheets exhibit remarkably strong PA signals under NIR laser illumination of 700 nm. In contrast, the GO nanosheets did not show any detectable PA signal at the same concentration and NIR illumination, possibly because of their low NIR absorption capability. Furthermore, the intensity of the PA signals depends on the concentration of the ME-LOGr nanosheets, suggesting that the ME-LOGr nanosheets can be used as NIR contrast agent for *in situ* NIR photoacoustic imaging. Since the strong NIR absorption of ME-LOGr nanosheets is almost independent of the wavelength in the NIR region, their NIR PA signal shows a similar trend of wavelength independence. Figure 7 shows that PA signals generated under 800 nm illumination are similar to those illuminated at 700 nm. This "wavelength-independent" characteristic is very different from other PA contrast agents, such as Au nanorods and Ag nanoplates, which are highly wavelength-dependent.[63]

CONCLUSIONS

In summary, for the first time, we demonstrated that graphene nanosheets can be directly fabricated from abundant and inexpensive graphite particles in a short one-pot nitronium oxidative reaction. The key is the utilization of microwave heating instead of traditional convective heating, which selectively and rapidly increases the local temperature of graphite particles thus leading to a unique thermodynamic effect. As a result, several positive outcomes are produced that steer the graphite oxidation processes toward direct fabrication of graphene nanosheets instead of GO nanosheets: (1) The

intercalation of nitronium ions into the inner parts of graphite particles is dramatically sped up. (2) A large amount of oxygen-containing groups (defects) are generated simultaneously, and they are randomly distributed across the entire graphene sheets. (3) Further oxidation of these defects or defect consumption reactions is more rapid than the pathways generating additional defects on the intact graphitic domains. (4) Finally, graphene nanosheets are directly and rapidly fabricated with the intrinsic properties of graphene largely retained.

This fabrication process involved no toxic metal compounds or reduction agents during the fabrication, and the product can be easily cleaned and purified. It is noteworthy that this method of fabricating nanosheets is different from all the approaches relying on GO *via* Hummers method or modified Hummers methods, in which strongly oxidative metallic compounds, such as $KMnO_4$, were required for the oxidation and other chemicals for the reduction of the produced GO. Trace amounts of metal ions and other chemicals involved in the oxidation and subsequent reduction processes may participate in unwanted toxic reactions, which could be detrimental to biological and other applications.[65,66] However, purification of GO is difficult due to its tendency to gel.[49] Therefore, extensive purification steps, which require large amount of solvents and long washing times, make the production of clean GO and rGO very time-consuming.[49] Another merit of the produced ME-LOGr nanosheets is that they can be directly dispersed into aqueous and other polar organic solvents without surfactants or stabilizing agents, allowing for the production of solutions of graphene nanosheets with "clean" surfaces. Most importantly, without the requirement for postreduction processes, the fabricated graphene nanosheets exhibit strong NIR absorption, high photothermal, and photoacoustic conversion efficiencies. Therefore, they possess great potential as nanocarriers to develop multifunctional drug delivery systems with "on demand' release and *in vivo* photoacoustic imaging capabilities for *in situ* evaluation of therapeutic effects and for tracking their long term fate.

MATERIALS AND METHODS

Materials. Synthetic graphite powder (20 μm) was purchased from Sigma Aldrich and used as received in all experiments. Concentrated sulfuric acid (98% H_2SO_4, ACS grade) and concentrated nitric acid (70% HNO_3, ACS grade) were purchased from Pharmco-AAPER and used as received. Deionized water (18.2 MΩ) (Nanopure water, Barnstead) was used to prepare all solutions and to rinse and clean the samples.

Experimental Procedures. *Fabrication of ME-LOGr nanosheets.* 20 mg of graphite are mixed with concentrated sulfuric acid and water in a round-bottom flask. The mixture is then swirled and cooled in an ice bath for approximately 5 min. Concentrated nitric acid is then added (different volume ratios of HNO_3:H_2SO_4:H_2O are given in the Table 1 below). The entire mixture is swirled and mixed for another 30 s and placed into a microwave reactor chamber (CEM Discover). The flask is connected to a reflux condenser that passes through the roof of the microwave oven *via* a port. The reaction mixture is subject to microwave irradiation (300 W) for 30 s. Subsequently, the reaction is quenched with 200 mL of deionized water, filtered through an alumina anodisc filter (0.02 μm pore size), and washed with 800 mL of deionized water. The cake on the membrane is then redispersed into water with 30 min of bath sonication. The dispersion obtained is then left undisturbed for five days to let the unexfoliated graphite particles precipitate out. The supernatant is carefully decanted, and this solution is stable for months in water without significant precipitation.

Control-A experiment. 100 mg of $KMnO_4$ is added to the ice-cooled acid mixture, as described above. After 30 s of microwave irradiation, the mixture is transferred to 200 mL of ice containing 5 mL of 35% H_2O_2 to quench the reaction. The entire content is then filtered through an alumina anodisc filter (0.02 μm pore size) and washed with 3 times 100 mL of diluted hydrochloric acid (4%), followed by repeatedly (8 times) washing with 100 mL of deionized water to remove all the acid and $KMnO_4$ residues, along with any byproducts. A colloidal graphene oxide (GO) solution is obtained by mild bath sonication (~30 min). Unexfoliated graphite powder can be removed by centrifugation at 4000 rpm for 20 min. The filtration and washing step in GO takes an entire day because of its paste-like character.

TABLE 1. Different Volume Ratio of HNO_3:H_2SO_4:H_2O

name	volume ratio (HNO_3:H_2SO_4:H_2O)	total volume (mL)
(1)	1:1:0	10
(2)	1:42:7	10
(3)	1:2.5:0.07	10
(4)	1:17.5:1.5	10
(5)	1:4:0	10

Control-B experiment. 100 mg of $KMnO_4$ is added to the ice-cooled 10 mL of concentrated sulfuric acid instead of acid mixture, and other experimental procedures are similar to control-A experiment.

Control-C experiment. 20 mg of graphite and acid mixture (No. 3 in Table 1) was heated at 85 °C for 4 h in water bath in a fume hood with the flask connected to a reflux condenser. After that, the washing procedure is followed similar to ME-LOGr nanosheets.

Material Characterization. The morphology of the graphene and GO samples were studied using a Nanoscope IIIa Multimode scanning probe microscope system (Digital Instruments, Bruker) with a J scanner operated in the "Tapping Mode". Micro-Raman Spectroscopy (Kaiser Optical Systems Raman Microprobe) equipped with a 785 nm solid-state diode laser was performed to measure the relative concentrations of nitronium ions formed *via* mixing concentrated HNO_3 and H_2SO_4 at different volume ratios. Spectra were obtained of these solutions held in a thin quartz cuvette. This instrument was also used to study the graphene and GO films deposited on an alumina filter membrane. XPS characterization was performed after depositing a layer of ME-LOGr nanosheets or GO onto a gold film (a 100 nm gold layer was sputter-coated on silicon with a 10 nm Ti adhesion layer). The thickness of the graphene or GO film on the gold substrates was roughly 30−50 nm. XPS spectra were acquired using a Thermo Scientific K-Alpha system with a monochromatic Al Kα X-ray source ($h\nu$ = 1486.7 eV), and data were analyzed using Casa XPS 2.3.15 software. Absorption spectra were recorded on a Cary 5000 UV−vis−NIR spectrophotometer in the double beam mode using a 1 cm quartz cuvette.

Photoacoustic characterization. A mechanically scanning photoacoustic system with a single acoustic transducer to collect the acoustic signals was employed, as described in detail previously.[67,68] A schematic of the system is shown in Figure S5 (Supporting Information). Briefly, pulsed light from an OPO laser

(Continuum, pulse duration: 4−6 ns, repetition rate: 20 Hz) was coupled into the phantom *via* an optical subsystem and generated acoustic signals. An acoustic transducer with 1 MHz nominal frequency (Valpey Fisher, Hopkinton, MA) was driven by a motorized rotator to receive acoustic signals over 360° at an interval of 3°. Thus a total of 120 measurements were performed for one planar scanning. The acoustic transducer was immersed in the water tank while the phantoms were placed at the center of the tank and illuminated by the laser. The acoustic signal was amplified by a pulser/receiver (GE Panametrics, Waltham, MA) and was then acquired by a high-speed PCI data acquisition board.

In these experiments, a solid cylindrical phantom with a diameter of 3 cm was prepared. The absorption and scattering coefficients were 0.01 and 1.0 mm^{-1} at ~700 and 800 nm, respectively. 3 μL of ME-LOGr nanosheets or GO with different concentrations were then put into three holes of 1.4 mm in diameter that were located in the center of the phantom. The phantom materials consisted of TiO_2 for scattering and India ink as an absorber with agar powder (1−2%) for solidifying the TiO_2 and India ink solution.

Conflict of Interest: The authors declare no competing financial interest.

Acknowledgment. This material is based upon work supported by the National Science Foundation under Grant CHE-0750201, CBET-0933966, MRI-1039828 (P.C. and H.H.), DMR 1006740 (E.G. and D.M.) and the J. Crayton Pruitt Family Endowment (H.J.).

Supporting Information Available: Digital photographs of stable ME-LOGr solutions in different solvents, statistical analysis of the ME-LOGr nanosheets for their lateral dimension and thickness, full Raman spectra of H_2SO_4/HNO_3 mixtures with different ratios for different concentrations of nitronium ions, and their detailed peak assignment of the Raman spectra, characterization of products obtained from varies control experiments, and the schematic drawing of the PAI system. These materials are available free of charge *via* the Internet at http://pubs.acs.org.

REFERENCES AND NOTES

1. Kosynkin, D. V.; Higginbotham, A. L.; Sinitskii, A.; Lomeda, J. R.; Dimiev, A.; Price, B. K.; Tour, J. M. Longitudinal Unzipping of Carbon Nanotubes to Form Graphene Nanoribbons. *Nature* **2009**, *458*, 872–875.
2. Chen, X.; Zhou, X. J.; Han, T.; Wu, J. Y.; Zhang, J. Y.; Guo, S. W. Stabilization and Induction of Oligonucleotide I-Motif Structure *via* Graphene Quantum Dots. *ACS Nano* **2013**, *7*, 531–537.
3. Ren, H. L.; Wang, C.; Zhang, J. L.; Zhou, X. J.; Xu, D. F.; Zheng, J.; Guo, S. W.; Zhang, J. Y. DNA Cleavage System of Nanosized Graphene Oxide Sheets and Copper Ions. *ACS Nano* **2010**, *4*, 7169–7174.
4. Yang, K.; Wan, J. M.; Zhang, S.; Tian, B.; Zhang, Y. J.; Liu, Z. The Influence of Surface Chemistry and Size of Nanoscale Graphene Oxide on Photothermal Therapy of Cancer Using Ultra-Low Laser Power. *Biomaterials* **2012**, *33*, 2206–2214.
5. Radovic, L. R.; Bockrath, B. On the Chemical Nature of Graphene Edges: Origin of Stability and Potential for Magnetism in Carbon Materials. *J. Am. Chem. Soc.* **2005**, *127*, 5917–5927.
6. Ohba, T.; Kanoh, H. Intensive Edge Effects of Nanographenes in Molecular Adsorptions. *J. Phys. Chem. Lett.* **2012**, *3*, 511–516.
7. Chou, S. S.; De, M.; Luo, J. Y.; Rotello, V. M.; Huang, J. X.; Dravid, V. P. Nanoscale Graphene Oxide (NGO) as Artificial Receptors: Implications for Biomolecular Interactions and Sensing. *J. Am. Chem. Soc.* **2012**, *134*, 16725–16733.
8. Pan, D. Y.; Zhang, J. C.; Li, Z.; Wu, M. H. Hydrothermal Route for Cutting Graphene Sheets into Blue-Luminescent Graphene Quantum Dots. *Adv. Mater.* **2010**, *22*, 734–738.
9. Li, Y.; Hu, Y.; Zhao, Y.; Shi, G. Q.; Deng, L. E.; Hou, Y. B.; Qu, L. T. An Electrochemical Avenue to Green-Luminescent Graphene Quantum Dots as Potential Electron-Acceptors for Photovoltaics. *Adv. Mater.* **2011**, *23*, 776–780.
10. Zhou, X. J.; Zhang, Y.; Wang, C.; Wu, X. C.; Yang, Y. Q.; Zheng, B.; Wu, H. X.; Guo, S. W.; Zhang, J. Y. Photo-Fenton Reaction of Graphene Oxide: A New Strategy to Prepare Graphene Quantum Dots for DNA Cleavage. *ACS Nano* **2012**, *6*, 6592–6599.
11. Hummers, W. S.; Offeman, R. E. Preparation of Graphitic Oxide. *J. Am. Chem. Soc.* **1958**, *80*, 1339.
12. Erickson, K.; Erni, R.; Lee, Z.; Alem, N.; Cannett, W. A. Z. Determination of the Local Chemical Structure of Graphene Oxide and Reduced Graphene Oxide. *Adv. Mater.* **2010**, *22*, 4467–4472.
13. Li, J.-L.; Kudin, K. N.; McAllister, M. J.; Prud'homme, R. K.; Aksay, I. A.; Car, R. Oxygen-Driven Unzipping of Graphitic Materials. *Phys. Rev. Lett.* **2006**, *96*, 176101.
14. Zhang, L.; Liang, J. J.; Huang, Y.; Ma, Y. F.; Wang, Y.; Chen, Y. S. Size-Controlled Synthesis of Graphene Oxide Sheets on a Large Scale Using Chemical Exfoliation. *Carbon* **2009**, *47*, 3365–3368.
15. Wang, D.; Wang, L.; Dong, X. Y.; Shi, Z.; Jin, J. Chemically Tailoring Graphene Oxides into Fluorescent Nanosheets for Fe3+ Ion Detection. *Carbon* **2012**, *50*, 2147–2154.
16. Luo, J. Y.; Cote, L. J.; Tung, V. C.; Tan, A. T. L.; Goins, P. E.; Wu, J. S.; Huang, J. X. Graphene Oxide Nanocolloids. *J. Am. Chem. Soc.* **2010**, *132*, 17667–17669.
17. Peng, J.; Gao, W.; Gupta, B. K.; Liu, Z.; Romero-Aburto, R.; Ge, L. H.; Song, L.; Alemany, L. B.; Zhan, X. B.; Gao, G. H.; *et al.* Graphene Quantum Dots Derived from Carbon Fibers. *Nano Lett.* **2012**, *12*, 844–849.
18. Tian, B.; Wang, C.; Zhang, S.; Feng, L. Z.; Liu, Z. Photothermally Enhanced Photodynamic Therapy Delivered by Nano-Graphene Oxide. *ACS Nano* **2011**, *5*, 7000–7009.
19. Robinson, J. T.; Tabakman, S. M.; Liang, Y. Y.; Wang, H. L.; Casalongue, H. S.; Vinh, D.; Dai, H. J. Ultrasmall Reduced Graphene Oxide with High Near-Infrared Absorbance for Photothermal Therapy. *J. Am. Chem. Soc.* **2011**, *133*, 6825–6831.
20. Zhang, M.; Bai, L. L.; Shang, W. H.; Xie, W. J.; Ma, H.; Fu, Y. Y.; Fang, D. C.; Sun, H.; Fan, L. Z.; Han, M.; *et al.* Facile Synthesis of Water-Soluble, Highly Fluorescent Graphene Quantum Dots as a Robust Biological Label for Stem Cells. *J. Mater. Chem.* **2012**, *22*, 7461–7467.
21. Xu, S. C.; Irle, S.; Musaev, D. G.; Lin, M. C. Quantum Chemical Study of the Dissociative Adsorption of OH and H_2O on Pristine and Defective Graphite (0001) Surfaces: Reaction Mechanisms and Kinetics. *J. Phys. Chem. C* **2007**, *111*, 1355–1365.
22. Liu, J.; Rinzler, A. G.; Dai, H. J.; Hafner, J. H.; Bradley, R. K.; Boul, P. J.; Lu, A.; Iverson, T.; Shelimov, K.; Huffman, C. B.; *et al.* Fullerene Pipes. *Science* **1998**, *280*, 1253–1256.
23. Ziegler, K. J.; Gu, Z. N.; Peng, H. Q.; Flor, E. L.; Hauge, R. H.; Smalley, R. E. Controlled Oxidative Cutting of Single-Walled Carbon Nanotubes. *J. Am. Chem. Soc.* **2005**, *127*, 1541–1547.
24. Kingston, H. M.; Haswell, S. J. *Microwave-Enhanced Chemistry: Fundamentals, Sample Preparation, and Applications*; American Chemical Society: Washington, D.C., 1997.
25. Kappe, C. O. Controlled Microwave Heating in Modern Organic Synthesis. *Angew. Chem., Int. Ed.* **2004**, *43*, 6250–6284.
26. Sun, T.; Fabris, S. Mechanisms for Oxidative Unzipping and Cutting of Graphene. *Nano Lett.* **2012**, *12*, 17–21.
27. Chiu, P. L.; Mastrogiovanni, D.; Wei, D.; Louis, C.; Jeong, M.; Yu, G.; Saad, P.; Flach, C. R.; Mendelsohn, R.; Garfunkel, E.; *et al.* Microwave- and Nitronium Ion- Enabled Rapid and Direct Production of Highly Conductive Low-Oxygen Graphene. *J. Am. Chem. Soc.* **2012**, *134*, 5850–5856.
28. Sun, X. M.; Luo, D. C.; Liu, J. F.; Evans, D. G. Monodisperse Chemically Modified Graphene Obtained by Density Gradient Ultracentrifugal Rate Separation. *ACS Nano* **2010**, *4*, 3381–3389.
29. Li, D.; Muller, M. B.; Gilje, S.; Kaner, R. B.; Wallace, G. G. Processable Aqueous Dispersions of Graphene Nanosheets. *Nat. Nanotechnol.* **2008**, *3*, 101–105.
30. Hernandez, Y.; Nicolosi, V.; Lotya, M.; Blighe, F. M.; Sun, Z. Y.; De, S.; McGovern, I. T.; Holland, B.; Byrne, M.; Gun'Ko, Y. K.; *et al.* High-Yield Production of Graphene by Liquid-Phase Exfoliation of Graphite. *Nat. Nanotechnol.* **2008**, *3*, 563–568.

31. Becerril, H. A.; Mao, J.; Liu, Z. F.; Stoltenberg, R. M.; Bao, Z.; Chen, Y. S. Evaluation of Solution-Processed Reduced Graphene Oxide Films as Transparent Conductors. *ACS Nano* **2008**, *2*, 463–470.
32. Bagri, A.; Mattevi, C.; Acik, M.; Chabal, Y. J.; Chhowalla, M.; Shenoy, V. B. Structural Evolution During the Reduction of Chemically Derived Graphene Oxide. *Nat. Chem.* **2010**, *2*, 581–587.
33. Eda, G.; Fanchini, G.; Chhowalla, M. Large-Area Ultrathin Films of Reduced Graphene Oxide as a Transparent and Flexible Electronic Materials. *Nat. Nanotechnol.* **2008**, *3*, 270–274.
34. Loh, K. P.; Bao, Q. L.; Eda, G.; Chhowalla, M. Graphene Oxide as a Chemically Tunable Platform for Optical Applications. *Nat. Chem.* **2010**, *2*, 1015–1024.
35. Park, S.; Ruoff, R. S. Chemical Methods for the Production of Graphene. *Nat. Nanotechnol.* **2009**, *4*, 217–224.
36. Chien, C. T.; Li, S. S.; Lai, W. J.; Yeh, Y. C.; Chen, H. A.; Chen, I. S.; Chen, L. C.; Chen, K. H.; Nemoto, T.; Isoda, S.; *et al.* Tunable Photoluminescence from Graphene Oxide. *Angew. Chem., Int. Ed.* **2012**, *51*, 6662–6666.
37. Eda, G.; Chhowalla, M. Chemically Derived Graphene Oxide: Towards Large-Area Thin-Film Electronics and Optoelectronics. *Adv. Mater.* **2010**, *22*, 2392–2415.
38. Eda, G.; Lin, Y. Y.; Mattevi, C.; Yamaguchi, H.; Chen, H. A.; Chen, I. S.; Chen, C. W.; Chhowalla, M. Blue Photoluminescence from Chemically Derived Graphene Oxide. *Adv. Mater.* **2010**, *22*, 505–509.
39. Zhu, S. J.; Tang, S. J.; Zhang, J. H.; Yang, B. Control the Size and Surface Chemistry of Graphene for the Rising Fluorescent Materials. *Chem. Commun.* **2012**, *48*, 4527–4539.
40. Moon, I. K.; Lee, J.; Ruoff, R. S.; Lee, H. Reduced Graphene Oxide by Chemical Graphitization. *Nat. Commun.* **2010**, *1*, 73.
41. Tung, V. T.; Allen, M. J.; Yang, Y.; Kaner, R. B. High-Throughput Solution Processing of Large-Scale Graphene. *Nat. Nanotechnol.* **2009**, *4*, 25–29.
42. Tuinstra, F.; Koenig, J. L. Raman Spectrum of Graphite. *J. Chem. Phys.* **1970**, *53*, 1126–1130.
43. Wang, H. L.; Robinson, J. T.; Li, X. L.; Dai, H. J. Solvothermal Reduction of Chemically Exfoliated Graphene Sheets. *J. Am. Chem. Soc.* **2009**, *131*, 9910–9911.
44. Niyogi, S.; Bekyarova, E.; Itkis, M. E.; Zhang, H.; Shepperd, K.; Hicks, J.; Sprinkle, M.; Berger, C.; Lau, C. N.; Deheer, W. A.; *et al.* Spectroscopy of Covalently Functionalized Graphene. *Nano Lett.* **2010**, *10*, 4061–4066.
45. Farmer, D. B.; Golizadeh-Mojarad, R.; Perebeinos, V.; Lin, Y. M.; Tulevski, G. S.; Tsang, J. C.; Avouris, P. Chemical Doping and Electron-Hole Conduction Asymmetry in Graphene Devices. *Nano Lett.* **2009**, *9*, 388–392.
46. Lotya, M.; Hernandez, Y.; King, P. J.; Smith, R. J.; Nicolosi, V.; Karlsson, L. S.; Blighe, F. M.; De, S.; Wang, Z.; McGovern, I. T.; *et al.* Liquid Phase Production of Graphene by Exfoliation of Graphite in Surfactant/Water Solutions. *J. Am. Chem. Soc.* **2009**, *131*, 3611–3620.
47. Li, Z. Y.; Zhang, W. H.; Luo, Y.; Yang, J. L.; Hou, J. G. How Graphene Is Cut Upon Oxidation? *J. Am. Chem. Soc.* **2009**, *131*, 6320–6321.
48. Chen, Z. Y.; Kobashi, K.; Rauwald, U.; Booker, R.; Fan, H.; Hwang, W. F.; Tour, J. M. Soluble Ultra-Short Single-Walled Carbon Nanotubes. *J. Am. Chem. Soc.* **2006**, *128*, 10568–10571.
49. Kim, F.; Luo, J. Y.; Cruz-Silva, R.; Cote, L. J.; Sohn, K.; Huang, J. X. Self-Propagating Domino-Like Reactions in Oxidized Graphite. *Adv. Funct. Mater.* **2010**, *20*, 2867–2873.
50. Marcano, D. C.; Kosynkin, D. V.; Berlin, J. M.; Sinitskii, A.; Sun, Z. Z.; Slesarev, A.; Alemany, L. B.; Lu, W.; Tour, J. M. Improved Synthesis of Graphene Oxide. *ACS Nano* **2010**, *4*, 4806–4814.
51. Edwards, H. G. M.; Fawcett, V. Quantitative Raman Spectroscopic Studies of Nitronium Ion Concentrations in Mixtures of Sulphuric and Nitric Acids. *J. Mol. Struct.* **1994**, *326*, 131–143.
52. Loughin, S.; Grayeski, R.; Fischer, J. E. Charge Transfer in Graphite Nitrate and the Ionic Salt Model. *J. Chem. Phys.* **1978**, *69*, 3740–3745.
53. Esteves, P. M.; Carneiro, J. W. D.; Cardoso, S. P.; Barbosa, A. G. H.; Laali, K. K.; Rasul, G.; Prakash, G. K. S.; Olah, G. A. Unified Mechanistic Concept of Electrophilic Aromatic Nitration: Convergence of Computational Results and Experimental Data. *J. Am. Chem. Soc.* **2003**, *125*, 4836–4849.
54. Han, T. H.; Huang, Y. K.; Tan, A. T. L.; Dravid, V. P.; Huang, J. X. Steam Etched Porous Graphene Oxide Network for Chemical Sensing. *J. Am. Chem. Soc.* **2011**, *133*, 15264–15267.
55. Shen, H.; Liu, M.; He, H. X.; Zhang, L. M.; Huang, J.; Chong, Y.; Dai, J. W.; Zhang, Z. J. Pegylated Graphene Oxide-Mediated Protein Delivery for Cell Function Regulation. *ACS Appl. Mater. Interfaces* **2012**, *4*, 6317–6323.
56. Yang, K.; Feng, L. Z.; Shi, X. Z.; Liu, Z. Nano-Graphene in Biomedicine: Theranostic Applications. *Chem. Soc. Rev.* **2013**, *42*, 530–547.
57. Yang, K.; Zhang, S. A.; Zhang, G. X.; Sun, X. M.; Lee, S. T.; Liu, Z. A. Graphene in Mice: Ultrahigh *in Vivo* Tumor Uptake and Efficient Photothermal Therapy. *Nano Lett.* **2010**, *10*, 3318–3323.
58. Yang, X.; Zhang, X.; Liu, Z.; Ma, Y.; Huang, Y.; Chen, Y. High-Efficiency Loading and Controlled Release of Doxorubicin Hydrochloride on Graphene Oxide. *J. Phys. Chem. C* **2008**, *112*, 17554–17558.
59. Zhang, L. M.; Wang, Z. L.; Lu, Z. X.; Shen, H.; Huang, J.; Zhao, Q. H.; Liu, M.; He, N. Y.; Zhang, Z. J. Pegylated Reduced Graphene Oxide as a Superior Ssrna Delivery System. *J. Mater. Chem. B* **2013**, *1*, 749–755.
60. Zhang, Y.; Yang, K.; Hong, H.; Engle, J.; Feng, L.; Theuer, C.; Barnhart, T.; Liu, Z.; Cai, W. *In Vivo* Targeting and Imaging of Tumor Vasculature with Radiolabeled, Antibody-Conjugated Nano-Graphene. *Med. Phys.* **2012**, *39*, 3950–3950.
61. Sun, X. M.; Liu, Z.; Welsher, K.; Robinson, J. T.; Goodwin, A.; Zaric, S.; Dai, H. J. Nano-Graphene Oxide for Cellular Imaging and Drug Delivery. *Nano Res.* **2008**, *1*, 203–212.
62. Yang, X. M.; Skrabalak, S. E.; Li, Z. Y.; Xia, Y. N.; Wang, L. H. V. Photoacoustic Tomography of a Rat Cerebral Cortex *in Vivo* with Au Nanocages as an Optical Contrast Agent. *Nano Lett.* **2007**, *7*, 3798–3802.
63. De la zerda, A.; Kim, J. W.; Galanzha, E. I.; Cambhir, S. S.; Zharov, V. P. Advanced Contrast Nanoagents for Photoacoustic Molecular Imaging, Cytometry, Blood Test and Photothermal Theranostics. *Contrast Media Mol. Imaging* **2011**, *6*, 346–369.
64. Yang, K.; Hu, L. L.; Ma, X. X.; Ye, S. Q.; Cheng, L.; Shi, X. Z.; Li, C. H.; Li, Y. G.; Liu, Z. Multimodal Imaging Guided Photothermal Therapy Using Functionalized Graphene Nanosheets Anchored with Magnetic Nanoparticles. *Adv. Mater.* **2012**, *24*, 1868–1872.
65. Jachak, A. C.; Creighton, M.; Qiu, Y.; Kane, A. B.; Hurt, R. H. Biological Interactions and Safety of Graphene Materials. *MRS Bull.* **2012**, *37*, 1307–1313.
66. Sanchez, V. C.; Jachak, A.; Hurt, R. H.; Kane, A. B. Biological Interactions of Graphene-Family Nanomaterials: An Interdisciplinary Review. *Chem. Res. Toxicol.* **2012**, *25*, 15–34.
67. Yin, L.; Wang, Q.; Zhang, Q. Z.; Jiang, H. B. Tomographic Imaging of Absolute Optical Absorption Coefficient in Turbid Media Using Combined Photoacoustic and Diffusing Light Measurements. *Opt. Lett.* **2007**, *32*, 2556–2558.
68. Zhang, Q. Z.; Liu, Z.; Carney, P. R.; Yuan, Z.; Chen, H. X.; Roper, S. N.; Jiang, H. B. Non-Invasive Imaging of Epileptic Seizures *in Vivo* Using Photoacoustic Tomography. *Phys. Med. Biol.* **2008**, *53*, 1921–1931.